Joint Communication and Sensing Design in Coal Mine Safety Monitoring: 3D Phase Beamforming for RIS-Assisted Wireless Networks

Tianhao Guo, *Member, IEEE*, Xianzhong Li, Muyu Mei, Zhaohui Yang, *Member, IEEE*, Jia Shi, *Member, IEEE*, Kai-Kit Wong, *Fellow, IEEE*, Zhaoyang Zhang, *Senior Member, IEEE*

***Abstract*—This paper investigates the resource allocation of a reconfigurable intelligent surface (RIS)-aided joint communication and sensing (JCAS) system in a coal mine scenario. In the JCAS system, an RIS is implemented at the corner of the zigzag tunnels to improve the complicated wireless environment, where ground obstacles frequently block direct links. In addition, a wireless backhaul base station with a limited energy budget is deployed in the depth of the mine to sense the target area and provide internet of things (IoT) services and communication services for users. Furthermore, a data center is placed on the ground to analyze the obtained data and route the communication data. Under this deployment, a joint optimization problem of RIS phase shift matrix, RIS element switches, and area sensing time is proposed. We aim to maximize the successful sensed bits under total completion time, and maximum transmit power constraints. In order to solve this problem, an iterative algorithm is proposed. The successive convex approximation (SCA) based algorithm is used for the RIS phase shift matrix optimization subproblem. For the sensing time optimization subproblem, the quadratic approximation method is proposed to optimize the number of area perceptions. The coordinate descent method is utilized to optimize the RIS element switches. Simulation results show that the energy efficiency is improved by up to 38%, and 7% increases the specific data size compared with the benchmark solutions.**

***Index Terms*—Energy efficiency, reconfigurable intelligent surface, joint communication and sensing, safety monitoring schedule.**

I. Introduction

This work was supported in part by Zhejiang Key R&D Program under Grant 2023C01021, National Key R&D Program of China under Grant 2020YFB1807101 and 2018YFB1801104, and National Natural Science Foundation of China under Grant U20A20158, 61725104 and 61825104.

Tianhao Guo is with the Department of Physical and Electronic Engineering, Shanxi University, Taiyuan, China, and also with the State Key Laboratory of Integrated Services Networks (ISN), Xidian University, China. (e-mail: tianhao_guo@sxu.edu.cn).

Xianzhong Li is with the Department of Physical and Electronic Engineering, Shanxi University, Taiyuan, China. (e-mail: 2843475772@qq.com).

Muyu Mei is with the State Key Laboratory of Integrated Services Networks, School of the Telecommunication Engineering, and the Guangzhou Institute, Xidian University, Xian 710071, China (e-mail: mei_muyu@163.com).

Zhaohui Yang is with the Department of Information Science and Electronic Engineering Zhejiang Key Laboratory of Information Processing Communication and Networking, Zhejiang University, Hangzhou, China, and also with the Zhejiang Laboratory, Hangzhou, China. (e-mail: zhaohui.yang@ucl.ac.uk). Zhaohui yang is the corresponding author.

Jia Shi is with the State Key Laboratory of Integrated Services Networks (ISN), Xidian University, China. (e-mail: jiashi@xidian.edu.cn).

Kai-Kit Wong is with the Department of Electronic and Electrical Engineering, University College London, UK. (e-mail: kai-kit.wong@ucl.ac.uk).

Zhaoyang Zhang is with the Zhejiang University, Hangzhou, China. (e-mail: zhzy@zju.edu.cn).

WITH the rapid development of wireless networks, spectrum resources are becoming congested. High-frequency bands are exploited and investigated to meet the increasing demand of wireless networks, including radar bands. Due to the similar properties of the occupied frequency bands, radar and communication systems have many overlaps in system models, channel characteristics, and signal processing design. Integrating radar and communication can improve efficiency (integration gain [1]) of resources, e.g., spectrum, energy, and device cost (also reducing weight for drones [2]).

Radar signals can be modulated, while wireless communication is also built based on identification and authentication. The integration of sensing and communication is not only an improvement or extension of existing communication technologies but also a paradigm revolution. As the neural system of animals, sensing the environment and transmitting information are two essential functions. By combining communication and sensing, human beings can build the neural system of the physical world and the intelligent world.

Millimeter wave (mmWave) bands have been officially adopted in fifth-generation (5G) cellular systems. Adopting high-frequency bands brings wide bandwidth and increases detection resolution [3] by more than two orders of magnitude (to 0.1mm or less) [4]. Moreover, the "pencil-like" [5] mmWave beams suffer from only a few multi-path target echoes, which means far less clutter interference. In other words, the future networks can clearly "see" the world. In the 6G era, the positioning accuracy is expected to be 10 cm (indoor) and 1 m (outdoor) [6]. With the large-scale deployment of cellular networks, there are increasing emerging sensing-enabled applications for future networks. Solid applications include high-resolution indoor positioning [7], navigation, and even high-resolution computational imaging, extending perception range beyond line-of-sight in vehicular networks.

Among those applications, coal mining is a vertical industrial application where 5G/6G networks are promising to land. The standard requirements of industrial networks are low latency [8]–[10], indoor positioning, large-scale connections, and low power consumption [11]. In addition to these typical requirements, the unique requirement of coal mining is safety monitoring. This is due to the three unique properties of coal mining: water seepage, goaves, and toxic and explosive gases.

- Firstly, electromagnetic waves in the mmWave bands and higher bands experience a severe loss, especially in an environment with high-humidity air. However, the

disadvantages of communication can be the advantages of perception. Once it is found that the radar echo in a specific area of the tunnel has an unknown loss, an unmanned vehicle can be sent to check.

- Secondly, the goaf is a "cavity" created by artificial excavation or natural geological movement, which can cause severe loss of properties and human lives. The spatial location of the goaves is concealed and randomly distributed. Besides, the roof collapse of the goaf is uneasy to be predicted. The JCAS system is able to predict the danger and effectively detect it. Moreover, once people and equipment fall into the goaf, the structure inside the goaf can be "seen" through electromagnetic inverse scattering imaging technology [12], so rescue can be carried out in time.

This paper considers a small battery-powered wireless backhaul JCAS base station that can transmit the sensory data to the data center for further processing. From the system design point of view, time-division sensing and communication integrated system [2] is more suitable for power constraint scenarios. In order to ensure the freshness of the sensory data, the interval (sensing phase) between two successive communication phases should be short. However, there should also be enough time for sensing to ensure data accuracy and to send the sensory and communication data. Hence, the tradeoff between the sensing and transmission phase with the constraints of sensing and communication demands was optimized in this paper.

Reconfigurable intelligent surface (RIS), as a candidate technology of 6G, is also promising to be applied in coal mines [13]–[18]. The reasons are: 1) interference can be controlled for RIS communications; 2) it is easy to implement and manage RIS in tunnels of coal mines; 3) RIS is an economical and green way [19] to transmit data through winding tunnels (multi-hop RIS [20]); 4) since each element can independently control the incident signal, by continuously adjusting the reflection characteristics, the receiver can obtain different echo signals, thereby obtaining more environmental information; 5) the high spreading loss and molecular absorption often limit [21] the signal transmission distance and coverage range of mmWave and THz bands, while massive multiple input multiple output (MIMO) [21] and multi-hop RIS [20] can help combat the distance issue; 6) if accident happens, some hops of the RIS may encode the information of the place and the reason of the accident in the frontier of the mine; 7) If multiple antennas are too close, it will reduce the resolution of perception and cause the loss of matrix rank. RIS can be utilized in a distributed multi-antenna system, which can be considered to increase the aperture of the radar.

Although the utilization of RIS in coal mines is beneficial, there are still some open issues regarding integration. Among these issues, we focus on two vital questions in this work.

- Question 1: Is time-division sensing and communication feasible for security checks in coal mines?
- Question 2: Is it feasible to use RIS to assist wireless communications in coal mines?

We are devoted to answering these two questions in this work, and the results are summarized in the following contributions of this work:

- The RIS-assisted JCAS system in the coal mine scenario is modeled, and the allocation strategy of sensing time and communication time is optimized. The simulation results show that the JCAS system can perceive as much sensory data as possible by reasonably allocating sensing and communication time in coal mines to ensure mine safety.
- RIS is deployed in the coal mine tunnels, and the RIS phase shift matrix is optimized to improve the communication rate. After the optimization of three dimensions (3D)-RIS, the energy efficiency is further improved, which verifies the feasibility of RIS-assisted communications in the coal mine tunnels.

The rest of this paper is organized as follows. Section II presents the related works of JCAS and RIS. Section III introduces the system model of this paper. Section IV provides the problem formulation. Simulation results are provided in Section V, and Section VI concludes this paper.

II. Related Works

A. Related Works on Safety Monitoring in Coal Mines

Safety monitoring of the tunnel environment needs a high sampling density of data, which needs to deploy many traditional sensors to different places and upload data on time. Usually, we tend to use wires to bridge sensing points to gather data at processing servers. However, wired networks are less scalable because sensors must be deployed as the tunnel advances. In contrast, wireless sensor networks (WSNs) are scalable for tunnel environments, and multi-hop routing is necessary for WSNs because direct wireless transmission is unfeasible in winding tunnels [22]. WSNs routing protocols and sensor nodes deployment have been studied in various cases [22], [23]. However, the cost of device deployment and maintenance for WSNs is still high, and WSNs are unable to integrate industrial network services directly into the coal mine.

Wireless electromagnetic wave attenuation characteristics for underground coal mines are studied in various cases (rock roughness [24], dust concentration), but this kind of research is only suitable for ultra-high frequency (300 MHz to 3 GHz). The performance of the MIMO system operating at 60 GHz (mmWave) is studied in the real-world underground gold mine [25] in Quebec, Canada. For a 2×2 MIMO system, the channel capacity can reach at least 4 bits/s/Hz.

Sensing is the foundation of mechanized and automated mining systems. 2D or 3D profiling visualization systems enabled by mmWave or laser have been implemented in underground and surface mines in Australia and South Africa decades ago [26]–[28]. By monitoring the 2D and 3D cloud images of mining vehicles [26], [27], tunnels and dig areas, automation and safety can be guaranteed to some extent. Those systems above have no communication functions.

TABLE I: List of Notations for Problem Formulation

Notations	Meanings
T	Data update time.
t	Communication time.
D_k	Total perceived data of the k_{th} area.
b_k	Perceptual number sequence.
N	Number of RIS units.
n	Background noises.
K	The number of target areas.
t_0	The basic sensing slot.
q_k	Probability of success for sensing k_{th} area.
ϵ	Perceived probability coefficient.
d_k	Distance from the BS to the target area.
M	Number of base station antennas.
b_{opt}	Optimal perceptual times sequence

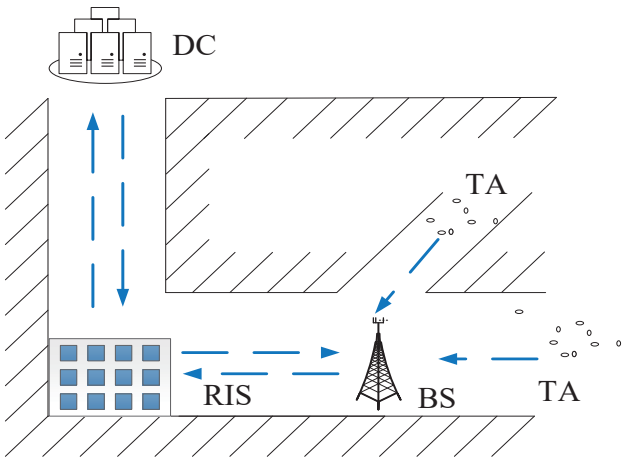

Fig. 1: System Model of Coal Mine Sensing and Communication.

B. Related Works on Integrated Sensing and Communication

From the signal processing point of view, the radar can modulate communication information on the radar electromagnetic waves such as pulse interval [29] and sidelobe of the MIMO radar beampattern [30]. On the other hand, the base station can also use its own reflected (echo) signals [31] to detect blockages such as walls because blockage can "modulate" signals by reflections. By collecting multi-path uplink signals from other devices with the aid of RIS, the pixel blocks (computational imaging) of the surroundings can be reconstructed [32], [33].

III. System Model

In this paper, we consider a wireless JCAS system, wherein data is sensed from a set $\mathbb{K}$ of K different target areas (TA), and the sensory data is transmitted to a data center (DC) with the help of a RIS to tackle the blockage of the cave, as shown in Fig. 1. The RIS has N reflecting elements and can be controlled through a diagonal matrix $\boldsymbol{\Theta} = \text{diag}(e^{j\theta_1}, \cdots, e^{j\theta_N}) \in \mathbb{C}^{N\times N}$ with $\theta_l \in [0, 2\pi]$ and $j = 1, \cdots, N$.

The notations and meanings appearing in the article are summarized in TABLE I. In order to sense different areas, the JCAS transmitter should be able to change the direction, and the beamforming vector is denoted by $\boldsymbol{\omega}$. The received signal at the DC is:

$$y = (\boldsymbol{g}^H + \boldsymbol{h}^H \boldsymbol{\Theta} \boldsymbol{G})\boldsymbol{\omega} + n, \tag{1}$$

where $\boldsymbol{g} \in \mathbb{C}^M$, $\boldsymbol{G} \in \mathbb{C}^{N\times M}$ and $\boldsymbol{h} \in \mathbb{C}^N$, denote the channel responses from the transmitter to the DC, from the transmitter to the RIS, and from the RIS to the DC, respectively. In (1), $n \sim \mathcal{CN}(0, \sigma^2)$ is the additive white Gaussian noise.

The JCAS system needs to sense K TAs and transmit the data repeatedly to ensure the freshness [2] of the sensory data. As shown in Fig. 2, a period T consists of a downloading phase (control and downloading data from DC to BS), a sensing phase, and an uploading phase (sensory data and communication data from BS to DC). Note that K TAs have different conditions and security requirements, so the sensing

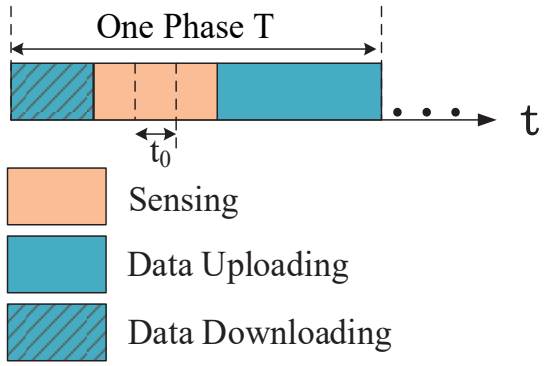

Fig. 2: Time Allocation of One Phase T.

priorities (sensing periods) may vary. The primary sensing slot of a TA is t_0, and the sensing duration t_k of k_{th} TA within a sensing phase is $b_k t_0$. The task completion probability of a TA in a sensing slot is [34]:

$$q_k = e^{-\epsilon d_k}, \tag{2}$$

where, ϵ_k is the perceived probability coefficient and d_k is the distance from the BS to the target area. The task completion probability of a TA in a sensing duration is:

$$P_k = 1 - (1 - q_k)^{b_k}. \tag{3}$$

The transmission (uploading and downloading) duration within a sensing phase is given by:

$$t = \frac{\sum_{k=1}^{K} P_k D_k + D_f}{B log_2(1 + \frac{\|\boldsymbol{g}^H + \boldsymbol{h}^H \boldsymbol{\Theta} \boldsymbol{G})\boldsymbol{\omega}\|^2}{\sigma^2})}, \tag{4}$$

where D_k is the data size of the k_{th} TA and B is the bandwidth. The size of uploading and downloading data is fixed to D_f. In order to formalize the problem, the mathematical expectation of the total data is used to approximate the sensed total data, expressed as $P_k \cdot D_k = P_k \cdot D_k + (1 - P_k) \cdot 0$.

Our objective is to jointly optimize the reflection coefficient matrix $\boldsymbol{\Theta}$ and sensing times b_k of the k_{th} TA to maximize the overall size of the sensory data under the data freshness requirements and the total power constraint $\boldsymbol{P}_{max}$. The problem can be formulated as follows:

$$\max_{\boldsymbol{b},\boldsymbol{\theta}} \quad \sum_{k=1}^{K} P_k D_k \tag{5}$$

$$\text{s.t.} \quad (\sum_{k=1}^{K} b_k) t_0 + t \leqslant T, \tag{5a}$$

$$P_k \geqslant Q_k, \quad k = 1, 2, 3 \ldots, K, \tag{5b}$$

$$\boldsymbol{\theta} \in [0, 2\pi], \tag{5c}$$

$$b_k \in N^+. \tag{5d}$$

The freshness constraint is guaranteed by (5a), where sensing duration $\sum_{k=1}^{K} b_k t_0$ plus transmitting duration are not allowed to exceed the period T to ensure the freshness of the sensory data. The task completion probability needs to satisfy the security requirements (Q_k in (5b)). That is, (5b)) guarantees the basic security requirement (Q_k) of each target area. On this basis, we try to improve the accuracy of sensing, so as to improve the security. For the sake of the sensing quality, we set a minimum successful sensing probability threshold Q_k for the BS. The power constraint is provided in (5c).

Batteries provide power for the BS and the RIS in the coal mine. When there are abundant RIS elements, the energy consumed by the RIS to regulate the phase is unignorable, even if the single RIS energy consumption is low. In order to further improve the energy efficiency, we add switch vectors to RIS elements and strive to find the optimal switch combination to further improve the energy efficiency.

The amplitude of RIS elements is controlled by the $\boldsymbol{x}$ vector, $\boldsymbol{x} = [x_1, \cdots, x_N]^T$, so as to realize the 3D control of RIS elements, The 3D-RIS optimization problem can be expressed by problem (6):

$$\max_{\boldsymbol{x}} \quad y = \boldsymbol{\omega}(\boldsymbol{g^H} + \boldsymbol{h^H X \Theta G}) + n \tag{6}$$

$$\text{s.t.} \quad x_1, \cdots, x_N \in \{0, 1\}, \tag{6a}$$

where, $\boldsymbol{X} = diag(\boldsymbol{x}^T) \in \mathbb{R}^N$. Since the problem has been formulated under the system model we presented in this section, we proceed to section IV.

IV. Problem Formulation

Problem (5) is nonconvex, and it is generally hard to obtain the global optimal solution, so (5) is divided into two sub-problems. Firstly, we optimize the RIS phase to maximize the channel gain. Secondly, we optimize the perceptual time allocation problem.

A. Phase Optimization

In this subsection, we are devoted to solving the first step. When $\boldsymbol{X}$ is an identity matrix, the phase shift matrix optimization problem can be expressed as:

$$\max_{\boldsymbol{\theta}} \quad y = \boldsymbol{\omega}(\boldsymbol{g^H} + \boldsymbol{h^H \Theta G}) + n \tag{7}$$

$$\text{s.t.} \quad \theta_j \in [0, 2\pi], j = 1, \cdots, N, \tag{7a}$$

where $\boldsymbol{\theta} = [e^{j\theta_1}, \cdots, e^{j\theta_N}]^T$. From the objective function (7) and the constraint in (7a), we observe that the optimal $\boldsymbol{\theta}$ is the one that maximizes the channel gain. Before optimizing $\boldsymbol{\theta}$, we notice that $h^H \boldsymbol{\Theta} = \boldsymbol{\theta}^T diag(\mathbf{h}^H)$. According to problem (6), the optimal $\boldsymbol{\theta}$ can be calculated by solving the following problem (8):

$$\max_{\boldsymbol{\theta}} \quad y = |\boldsymbol{g} + \boldsymbol{U^H v}|^2 \tag{8}$$

$$\text{s.t.} \quad |\boldsymbol{v}_j| = 1, j = 1, \cdots, N \tag{8a}$$

where, $\mathbf{U} = \text{diag}(\mathbf{h}^H)\mathbf{G}$ and $\boldsymbol{v} = \boldsymbol{\theta}^*$. This paper uses the successive convex approximation (SCA) method to optimize the problem (8), and the alternating optimization algorithm is the comparison algorithm.

Under the SCA approach, problem (8) can be approximated as:

$$\max_{\boldsymbol{\theta}} \quad 2R(\boldsymbol{g} + \boldsymbol{U}^H \boldsymbol{v}^{(j-1)})^H \boldsymbol{U}^H \boldsymbol{v}^j) - |\boldsymbol{g} + \boldsymbol{U}^H \boldsymbol{v}^{(j-1)}|^2 \tag{9}$$

$$\text{s.t.} \quad |\boldsymbol{v}_j| = 1, j = 1, \cdots, N. \tag{9a}$$

Lemma 1: In problem (9), the optimal solution is:

$$\boldsymbol{v}_{opt} = e^{-j\angle(\boldsymbol{U}(\boldsymbol{g} + \boldsymbol{U}^H \boldsymbol{v}^{(j-1)}))}. \tag{10}$$

Proof: $\angle(\boldsymbol{U}(\boldsymbol{g} + \boldsymbol{U}^H \boldsymbol{v}^{(j-1)}))$ denotes the phase of $(\boldsymbol{U}(\boldsymbol{g} + \boldsymbol{U}^H \boldsymbol{v}^{(j-1)})$. When the phase of $(\boldsymbol{g} + \boldsymbol{U}^H \boldsymbol{\theta}^{(n-1)})\boldsymbol{U}^H$ and $\boldsymbol{v}$ are opposite, the value of the objective function can be optimized, and Eq. (10) is the optimal solution. The SCA algorithm for solving the problem (8) is summarized in Algorithm 1.

For comparison, we alternatively optimize the phase of one element in RIS and fix the phase angle of other elements. This method decomposes the multi-dimensional optimization problem into multiple one-dimensional optimization problems to simplify the calculation. The detailed steps are shown in Algorithm 2.

Algorithm 1 SCA Method

Initialize $\boldsymbol{v}^{(0)}$, set iternumber $n = 1$.
repeat
  set $\boldsymbol{v}^{(j)} = e^{-j\angle(\boldsymbol{U}(\boldsymbol{g} + \boldsymbol{U}^H \boldsymbol{\theta}^{(j-1)}))}$, and, $j = j + 1$.
until the obiective value converges, $\boldsymbol{\theta} = (\boldsymbol{v}^{(j)})^*$.

Algorithm 2 Alternating Optimization Algorithm

Initialize $\theta_j = 0$, $j = 1 : N$.
repeat
  for $j = 1, \cdots, N$
    $\theta_j = argmax(y)$.
  endfor
until the obiective value converges.

B. Sensing Time Optimization

There are multiple target areas, and the size of sensory data in each TA varies for the coal mine scenario. Each TA's perceived probability needs to cater for the probability constraint due to different perceived priorities. The system's optimal sensing time allocation strategy needs to be obtained first.

As observed, problem (5) is a non-convex problem, which needs to be further transformed into a convex problem to be

solved. This paper uses the Taylor quadratic approximation method to solve the relaxation problem corresponding to the original integer programming problem for the perceptual time allocation problem. Replacing (2) into objective function in problem (5), we can obtain expression (11):

$$y = \sum_{k=1}^{K} [1 - (1 - q_k)^{b_k}] \cdot D_k. \tag{11}$$

Then, we let $Q_k = 1 - q_k$ and the objective function can be rewritten as $y = \sum_{k=1}^{K} [1 - {Q_k}^{b_k}] \cdot D_k$. Furthermore, the objective function is expanded to $y = \sum_{k=1}^{K} D_k - \sum_{k=1}^{K} {Q_k}^{b_k} \cdot D_k$ and $\sum_{k=1}^{K} D_k$ is the fixed value. Let $y_1 = \sum_{k=1}^{K} {Q_k}^{b_k} \cdot D_k$, y_1 becomes the new objective function. According to the Taylor expansion $a^x = \sum_{n=0}^{N} (xlna)^n/n!$, the objective function can be approximated as $y_1 = \sum_{k=1}^{K} [1 + b_k lnQ_k + (b_k lnQ_k)^2/2] \cdot D_k$. Let $y_2 = \sum_{k=1}^{K} [b_k lnQ_k + (b_k lnQ_k)^2/2] \cdot D_k$, the optimization problem (12) is obtained by expressing y_2 in matrix form:

$$\min_{\mathbf{b}} \quad y_2 = \mathbf{a}^T \cdot \mathbf{b} + \mathbf{b}^T \cdot \mathbf{A} \cdot \mathbf{b} \tag{12}$$

$$\text{s.t.} \quad Q_k \leqslant P_k \tag{12a}$$

$$t + \sum_{k=1}^{K} b_k t_0 \leqslant T \tag{12b}$$

where $\mathbf{a} = [D_1 lnQ_1, \cdots, D_K lnQ_K]^T$, $\mathbf{b} = [b_1, \cdots, b_K]^T$ and $\mathbf{A} = diag[(lnQ_1)^2 \cdot D_1/2, \cdots, (lnQ_K)^2 \cdot D_K/2]$. From problem (12), we observe that the non-convex problem is transformed into a convex problem. Then, we obtain the optimal solution of the original problem by comparing the objective function value of the integer solution near the optimal solution of the relaxation problem. The optimization method for solving the problem (12) is summarized in Algorithm 3.

For comparison, the enumeration method is used to solve this integer programming problem. The specific iterative process is summarized in Algorithm 4. Besides, for the convex optimization process in algorithms 3 and 4, we utilize the interior-point method.

Algorithm 3 The Quadratic Approximation Method

Initialze, $b_k = 1$, $k = 1, \cdots$,K, $\mathbf{b} = [b_1, \cdots, b_K]^T$,
$\mathbf{b} = argmin(y_2)$, $\mathbf{bl} = \lfloor \mathbf{b} \rfloor$, $\mathbf{bh} = \lceil \mathbf{b} \rceil$, $\mathbf{bA} = [\mathbf{bl}, \mathbf{bh}]$.
for $j_1, \cdots, j_K \in \{1, 2\}$ **do**
while $t + \sum_{k=1}^{K} b_k * t_0 < T$ **and** $Q_k \leqslant P_k$ **do**
$b_1 = \mathbf{bA}(1, j_1)$,
$\vdots$
$b_K = \mathbf{bA}(K, j_K)$.
if $y_{before} \leqslant y_{update}$
$y = y_{update}$
Update **b**
endif
endwhile
endfor
output $\mathbf{b}_{opt}$=**b**.

Algorithm 4 Enumeration Method

Initialize $b_k = 1$, $k = 1, \cdots$,K, $b_{max} = max\{b_1, \cdots, b_K\}$,
$\mathbf{b} = [b_1, \cdots, b_K]^T$.
repeat
Update the maximum value of perception times
$bmax = \lfloor (T - t)/t0 - K + 1 \rfloor$.
for $b_1, \cdots, b_K \in \{1, \cdots, b_{max}\}$ **do**
while $t + \sum_{k=1}^{K} b_k * t_0 < T$ **and** $Q_k \leqslant P_k$ **do**
if $y_{before} \leqslant y_{update}$
$y = y_{update}$
Update **b**
endwhile
endfor
until Objective value converges.

C. Optimization Analysis of 3D-RIS.

The coordinate descent method is utilized for the problem (6). Detailed steps of this method are presented in the following.

First, we adopt a utility function:

$$y_{m_i} = y_{\boldsymbol{x}_i} - y_{\boldsymbol{x}}, \tag{13}$$

where $\boldsymbol{x}_i$ represents the switching sequence after the update, and $\boldsymbol{x}$ represents the switching sequence before the update. The updating rule of the switch sequence is given by (14).

$$\boldsymbol{x}_i = [x_1, \cdots, x_i \oplus 1, \cdots, x_N]^T. \tag{14}$$

In the iteration process, we will change the switch state of the ${i^*}_{th}$ element, where, i^* is derived as:

$$i^* = \arg\max_i \{\mathbf{y}_m\}, \tag{15}$$

where $\mathbf{y}_m = [y_{m_1}, \cdots, y_{m_N}]^T$. The algorithm for solving the problem (6) is summarized in Algorithm 5. Finally, the algorithm to solve the problem (5) is summarized in Algorithm 6. The interior-point method is used in the iterative process.

D. Complexity Analysis

According to Algorithm 1, to solve the problem (8), the complexity lies in computing the next iteration point $\boldsymbol{v}_j$, which involves the complexity of $\mathcal{O}(N)$. Algorithm 2 is dominated by the complexity of the alternating process, where the number of iterations increases sharply and is represented by S, so the complexity is $\mathcal{O}(NS)$. In Algorithm 3, the complexity of the quadratic approximation method for solving the problem (12) is $\mathcal{O}(2^N)$. N represents the number of variables, and each variable can be converted between two values. According to Algorithm 4, all states of the variable need to be traversed one by one. N variables require close to N^N iterations. So, the enumeration method in Algorithm 4 involves the complexity of $\mathcal{O}(N^N)$. The number of iterations decreases gradually in solving the problem (6). N variables require $N!$ iterations. So,

This article has been accepted for publication in IEEE Internet of Things Journal. This is the author's version which has not been fully edited and content may change prior to final publication. Citation information: DOI 10.1109/JIOT.2023.3242340

Algorithm 5 Coordinate Descent Method

Initialize $\boldsymbol{x} = [1, \cdots, 1]^T$, $\mathbf{y}_m = [y_{m_1}, \cdots, y_{m_N}]^T$
repeat
  for $i = 1 : N$
    $\boldsymbol{x}_i = [x_1, \cdots, x_i \oplus 1, \cdots, x_N]^T$,
    Calculation $y_{m_i} = y_{\boldsymbol{x}_i} - y_{\boldsymbol{x}}$
  endfor
    Update $i^* = \underset{i}{\operatorname{argmax}} \{\mathbf{y}_m\}$
  if $y_{x_{i^*}} > 0$
    Update $\boldsymbol{x} = [x_1, \cdots, x_{i^*} \oplus 1, \cdots, x_N]^T$
until Objective value converges.

Algorithm 6 Iterative Optimization for Problem (5)

Initialize $(\boldsymbol{\theta_{(0)}}, \boldsymbol{b_{(0)}}, \boldsymbol{x_{(0)}})$, Set iteration number n=1.
repeat
  Given $\boldsymbol{\theta_{(n-1)}}$, the optimized $\boldsymbol{\theta}$ is obtained by Algorithm 1 and denoted by $\boldsymbol{\theta_{(n)}}$.
  Given $\boldsymbol{\theta_{(n)}}$ and $\boldsymbol{x_{(n-1)}}$, the optimization problem (6) is solved by using Algorithm 5 and the solution is denoted by $\boldsymbol{x_{(n)}}$.
  Given $\boldsymbol{\theta_{(n)}}$, $\boldsymbol{x_{(n)}}$ and $\boldsymbol{b_{(n-1)}}$, we solve the optimization problem (5) according Algorithm 3.
  Set $n = n + 1$.
until The objective value converges.

TABLE II: Parameter Settings

Number	Application	Numerical	Unit
1	BS transmit power	50	dBm
2	Background noise power	-104	dBm
3	Bandwidth	1	MHz
4	Circuit power of the DC	39	dBm
5	Circuit power of BS	80	dBm
6	Power of a RIS element	10	dBm

the complex for the coordinate descent method in Algorithm 5 is $\mathcal{O}(N!)$.

V. Simulation Results and Discussion

This section provides the simulation results to verify the theoretical findings. The parameter settings [35] are summarized in TABLE II.

A. Phase Shift Matrix Optimization

This experiment uses the iterative method based on SCA to solve the RIS problem (8). The $\boldsymbol{\theta}$ in the experiment are set to random values, all one and all zero. The variation curves between the normalized channel gain value and the number of iterations are shown in Fig. 3, where the normalized channel gain represents the ratio of channel gain to the noise power, denoted by $|g + U^H v|^2/\sigma^2$.

As observed in Fig. 3, Algorithm 1 converges within ten iterations. In addition, we compare the SCA method with the alternative optimization method. The convergence curves of the alternating optimization and the SCA methods are shown

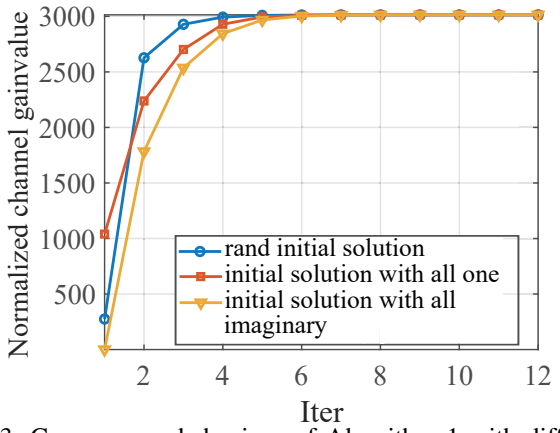

Fig. 3: Convergence behaviour of Algorithm 1 with different initial solutions.

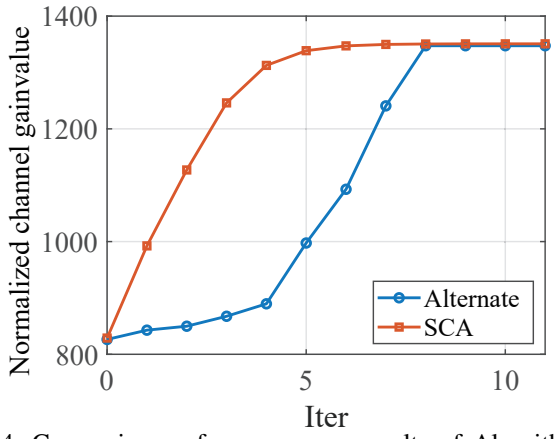

Fig. 4: Comparisons of convergence results of Algorithms 1 and 2.

in Fig. 4. In Fig. 4, Alternate means the objective value by utilizing the alternating optimization method. The horizontal coordinate corresponding to the alternating optimization in Fig. 4 is the number of updates of the objective function values rather than the number of iterations. We can see that after a finite number of iterations, two methods have converged, and the optimal function value is stable. However, alternative optimizations require more iterations to converge.

B. Perceptual Time Optimization

We show the results of Algorithm 3 and 4 in Figs. 5 and 6, respectively. In Fig. 5 and 6, before optimize means the objective value with random solution, while after optimize means the objective value with the optimal solution. In both figures, we show the objective values with various random settings. According to these two figures, we can find that the optimization of Algorithm 3 and 4 is correct.

In Fig. 5, we compare the optimization results of 10 tests. K is fixed as 5, and the objective function is the perceived total data. The total data after optimization is significantly larger than that before optimization. According to Algorithm 3, the optimal solution is feasible.

Fig. 6 compares function values before and after optimization using the enumeration method similar to Fig. 5. The

This article has been accepted for publication in IEEE Internet of Things Journal. This is the author's version which has not been fully edited and content may change prior to final publication. Citation information: DOI 10.1109/JIOT.2023.3242340

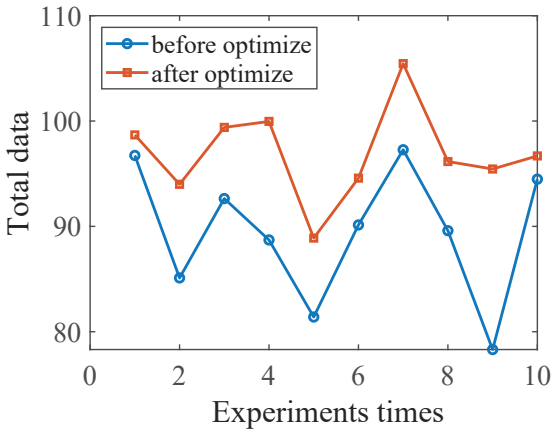

Fig. 5: Optimization results of Algorithm 3 versus multiple simulation times.

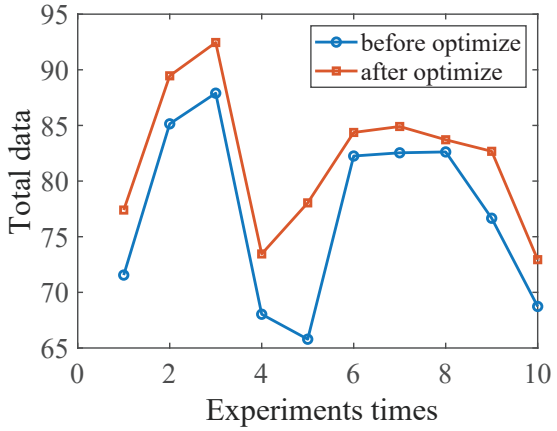

Fig. 6: Optimization results of Algorithm 4 versus multiple simulation times.

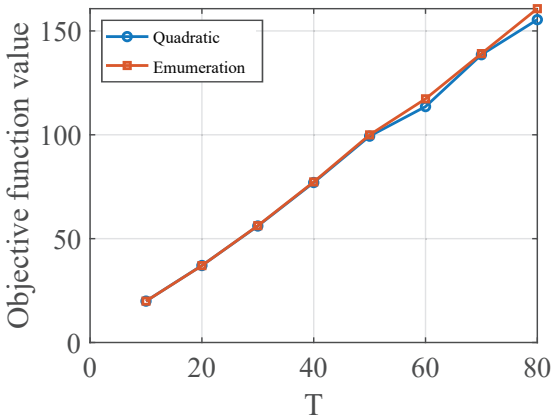

Fig. 7: Convergence comparison of two methods with different T.

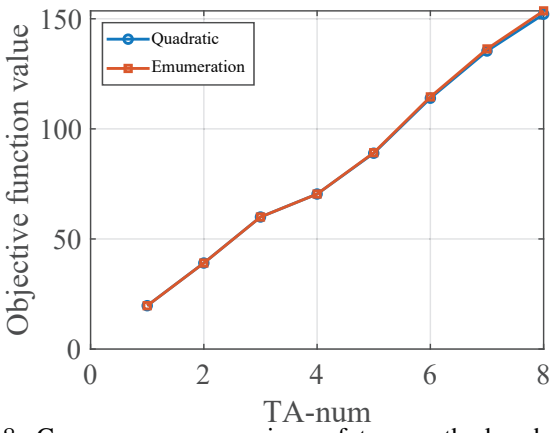

Fig. 8: Convergence comparison of two methods when the number of regions to be perceived is different.

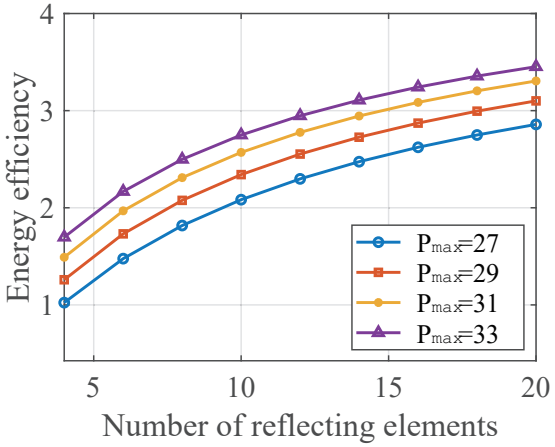

Fig. 9: Relationship between energy efficiency and RIS element number under different power.

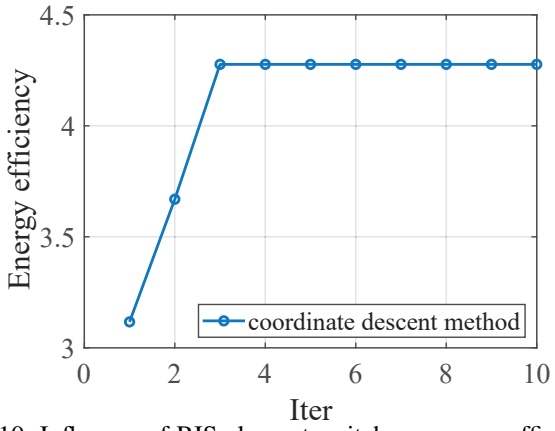

Fig. 10: Influence of RIS element switch on energy efficiency.

objective function value increases obviously after optimization. Therefore, the feasibility of the enumeration method is verified.

Fig. 7 shows how the perceived data changes as the data update time T varies for the quadratic approximation and enumeration methods. Here, for precise comparison, we set K as 8. There is almost no difference between the convergence results of the two methods because the quadratic approximation method approximates the original function. With the increase of T, there might be some errors.

Fig. 8 shows the perceived data versus the area perception times, where we let $T = 20 \times K$ based on experience. From this figure, we notice that the two methods almost converge to the same result, similar to Fig. 7. Thus, we verify that the quadratic approximation method can solve the problem (12) with low complexity.

Fig. 9 shows the curves of the energy efficiency (defined as the ratio of spectral efficiency over power consumption) and the number of RIS elements under various values of powers. It can be seen from Fig. 9 that the energy efficiency increases significantly with the increase of power and the number of RIS elements. Simultaneously, with the increase of RIS elements, the energy consumption for RIS is also higher.

Furthermore, we improve energy efficiency by turning off some elements. We set the RIS element to 100 and use the coordinate descent method to optimize the RIS element switches. The simulation results are shown in Fig. 10. We can see that the algorithm has reached convergence, and the energy efficiency has improved. This result shows that the energy consumed by RIS to regulate the phase can not be ignored when there are many RIS elements. We can improve energy efficiency by finding the optimal RIS element switching sequence.

VI. Conclusion

In this paper, we investigate the problem of resource allocation in the RIS-assisted coal mine JCAS system. RIS phase shift matrix, areas sensing times, and RIS element switch matrix are jointly optimized to sense as much secure data as possible while meeting the maximum data update time, maximum power, minimum area sensing demands, and unit-modulus constraints. In order to solve this problem, we use the SCA-based iterative algorithm to optimize the RIS phase shift matrix and the Taylor quadratic approximation method to optimize the times of area perception. Simulation results show that time-division sensing and communication are feasible for security checks, and using RIS to assist wireless communication in the coal mine is feasible.

References

[1] Y. Cui, F. Liu, X. Jing, and J. Mu, "Integrating sensing and communications for ubiquitous iot: Applications, trends and challenges," *arXiv preprint arXiv:2104.11457*, 2021.

[2] S. Zhang, H. Zhang, L. Song, Z. Han, and H. V. Poor, "Sensing and communication tradeoff design for aoi minimization in a cellular internet of uavs," in *ICC 2020 - 2020 IEEE International Conference on Communications (ICC)*, 2020, pp. 1–6.

[3] C. Wang, F. Lin, T. Liu, Z. Liu, Y. Shen, Z. Ba, L. Lu, W. Xu, and K. Ren, "mmphone: Acoustic eavesdropping on loudspeakers via mmwave-characterized piezoelectric effect," in *IEEE INFOCOM 2022 - IEEE Conference on Computer Communications(IEEE INFOCOM)*, 2022, pp. 820–829.

[4] M. Vogt, J. Opretzka, and H. Ermert, "Synthetic aperture focusing technique for high-resolution imaging of surface structures with high-frequency ultrasound," in *2009 IEEE International Ultrasonics Symposium(IEEE IUS)*, 2009, pp. 1514–1517.

[5] F. Liu, C. Masouros, A. P. Petropulu, H. Griffiths, and L. Hanzo, "Joint radar and communication design: Applications, state-of-the-art, and the road ahead," *IEEE Transactions on Communications*, vol. 68, no. 6, pp. 3834–3862, 2020.

[6] X. You, C.-X. Wang, J. Huang, X. Gao, Z. Zhang, M. Wang, Y. Huang, C. Zhang, Y. Jiang, J. Wang *et al.*, "Towards 6g wireless communication networks: Vision, enabling technologies, and new paradigm shifts," *Science China Information Sciences*, vol. 64, no. 1, pp. 1–74, 2021.

[7] S. Piao, Z. Ba, L. Su, D. Koutsonikolas, S. Li, and K. Ren, "Automating csi measurement with uavs: from problem formulation to energy-optimal solution," in *IEEE INFOCOM 2019 - IEEE Conference on Computer Communications(IEEE INFOCOM)*, 2019, pp. 2404–2412.

[8] Q. Wu, Y. Zhao, Q. Fan, P. Fan, J. Wang, and C. Zhang, "Mobility-aware cooperative caching in vehicular edge computing based on asynchronous federated and deep reinforcement learning," *IEEE Journal of Selected Topics in Signal Processing*, pp. 1–16, 2022.

[9] Y. Ye, L. Shi, X. Chu, G. Lu, and S. Sun, "Mutualistic cooperative ambient backscatter communications under hardware impairments," *IEEE Transactions on Communications*, vol. 70, no. 11, pp. 7656–7668, 2022.

[10] Q. Wu, S. Shi, Z. Wan, Q. Fan, P. Fan, and C. Zhang, "Towards v2i age-aware fairness access: A dqn based intelligent vehicular node training and test method," *arXiv preprint arXiv:2208.01283*, 2022.

[11] Y. Ye, L. Shi, X. Chu, R. Q. Hu, and G. Lu, "Resource allocation in backscatter-assisted wireless powered mec networks with limited mec computation capacity," *IEEE Transactions on Wireless Communications*, vol. 21, no. 12, pp. 10 678–10 694, 2022.

[12] X. Tong, Z. Zhang, Y. Zhang, Z. Yang, C. Huang, K.-K. Wong, and M. Debbah, "Environment sensing considering the occlusion effect: A multi-view approach," *IEEE Transactions on Signal Processing*, vol. 70, pp. 3598–3615, 2022.

[13] K. Yang, Y. Shi, Y. Zhou, Z. Yang, L. Fu, and W. Chen, "Federated machine learning for intelligent iot via reconfigurable intelligent surface," *IEEE Network*, vol. 34, no. 5, pp. 16–22, 2020.

[14] M. Fu, Y. Zhou, Y. Shi, and K. B. Letaief, "Reconfigurable intelligent surface empowered downlink non-orthogonal multiple access," *IEEE Transactions on Communications*, vol. 69, no. 6, pp. 3802–3817, 2021.

[15] Y. Xiu, J. Zhao, W. Sun, M. D. Renzo, G. Gui, Z. Zhang, and N. Wei, "Reconfigurable intelligent surfaces aided mmwave noma: Joint power allocation, phase shifts, and hybrid beamforming optimization," *IEEE Transactions on Wireless Communications*, vol. 20, no. 12, pp. 8393–8409, 2021.

[16] W. Ni, Y. Liu, Y. C. Eldar, Z. Yang, and H. Tian, "Star-ris integrated nonorthogonal multiple access and over-the-air federated learning: Framework, analysis, and optimization," *IEEE Internet of Things Journal*, vol. 9, no. 18, pp. 17 136–17 156, 2022.

[17] Z. Yang, M. Chen, W. Saad, W. Xu, M. Shikh-Bahaei, H. V. Poor, and S. Cui, "Energy-efficient wireless communications with distributed reconfigurable intelligent surfaces," *IEEE Transactions on Wireless Communications*, vol. 21, no. 1, pp. 665–679, 2022.

[18] X. U. Yongjun, Z. Yang, C. Huang, Y. Chau, and G. Gui, "Resource allocation for two-tier ris-assisted heterogeneous noma networks," *ZTE Communications*, vol. 20, no. 1, p. 12, 2022.

[19] C. Huang, A. Zappone, G. C. Alexandropoulos, M. Debbah, and C. Yuen, "Reconfigurable intelligent surfaces for energy efficiency in wireless communication," *IEEE Transactions on Wireless Communications*, vol. 18, no. 8, pp. 4157–4170, 2019.

[20] C. Huang, Z. Yang, G. C. Alexandropoulos, K. Xiong, L. Wei, C. Yuen, and Z. Zhang, "Hybrid beamforming for ris-empowered multi-hop terahertz communications: A drl-based method," in *2020 IEEE Globecom Workshops (GC Wkshps)*, 2020, pp. 1–6.

[21] I. F. Akyildiz, C. Han, and S. Nie, "Combating the distance problem in the millimeter wave and terahertz frequency bands," *IEEE Communications Magazine*, vol. 56, no. 6, pp. 102–108, 2018.

[22] M. Li and Y. Liu, "Underground coal mine monitoring with wireless sensor networks," *ACM Transactions on Sensor Networks (TOSN)*, vol. 5, no. 2, pp. 1–29, 2009.

[23] L. Muduli, P. K. Jana, and D. P. Mishra, "A novel wireless sensor network deployment scheme for environmental monitoring in longwall coal mines," *Process Safety and Environmental Protection*, vol. 109, pp. 564–576, 2017.

[24] X. Xusheng, M. Kun, M. Hongwei, S. Wanfeng, and F. Hongwei, "Analysis of wireless electromagnetic wave propagation mechanism for coal mine rescue robot," in *2018 IEEE International Conference on Real-time Computing and Robotics (RCAR)*, 2018, pp. 64–67.

[25] I. Ben Mabrouk, J. Hautcoeur, L. Talbi, M. Nedil, and K. Hettak, "Feasibility of a millimeter-wave mimo system for short-range wireless communications in an underground gold mine," *IEEE Transactions on Antennas and Propagation*, vol. 61, no. 8, pp. 4296–4305, 2013.

[26] G. Brooker, J. Martinez, and R. Hennessey, "Millimetre wave radar imaging of mining vehicles," in *The 7th European Radar Conference(EuRAD)*, 2010, pp. 284–287.

[27] G. Brooker, E. Widzyk-Capehart, S. Scheding, R. Hennessy, and C. Lobsey, "Millimetre wave radar visualisation in mines," in *2007 European Radar Conference (EuRAD 2007)*, 2007, pp. 417–420.

[28] M. Leingartner, J. Maurer, G. Steinbauer, and A. Ferrein, "Evaluation of sensors and mapping approaches for disasters in tunnels," in *2013 IEEE International Symposium on Safety, Security, and Rescue Robotics (SSRR)*, 2013, pp. 1–7.

[29] R. M. Mealey, "A method for calculating error probabilities in a radar communication system," *IEEE Transactions on Space Electronics and Telemetry*, vol. 9, no. 2, pp. 37–42, 1963.

[30] A. Hassanien, M. G. Amin, Y. D. Zhang, and F. Ahmad, "Dual-function radar-communications: Information embedding using sidelobe control

and waveform diversity," *IEEE Transactions on Signal Processing*, vol. 64, no. 8, pp. 2168–2181, 2016.

[31] C. Jiao, Z. Zhang, C. Zhong, X. Chen, and Z. Feng, "Millimeter wave communication with active ambient perception," *IEEE Transactions on Wireless Communications*, vol. 18, no. 5, pp. 2751–2764, 2019.

[32] J. Yao, Z. Zhang, X. Shao, C. Huang, C. Zhong, and X. Chen, "Concentrative intelligent reflecting surface aided computational imaging via fast block sparse bayesian learning," in *2021 IEEE 93rd Vehicular Technology Conference (VTC2021-Spring)*, 2021, pp. 1–6.

[33] Y. Tao and Z. Zhang, "Distributed computational imaging with reconfigurable intelligent surface," in *2020 International Conference on Wireless Communications and Signal Processing (WCSP)*, 2020, pp. 448–454.

[34] S. Zhang, H. Zhang, L. Song, Z. Han, and H. V. Poor, "Sensing and communication tradeoff design for aoi minimization in a cellular internet of uavs," in *ICC 2020 - 2020 IEEE International Conference on Communications (ICC)*, 2020, pp. 1–6.

[35] M. Chen, Z. Yang, W. Saad, C. Yin, H. V. Poor, and S. Cui, "A joint learning and communications framework for federated learning over wireless networks," *IEEE Transactions on Wireless Communications*, vol. 20, no. 1, pp. 269–283, 2021.

Tianhao Guo (Member, IEEE) received the PhD degree from School of Electronic Engineering and Computer Science, Queen Mary University of London, London, UK in 2020. He is currently a lecturer in Shanxi University. He is also the postdoctoral research associate with the National Key Laboratory of Integrated Services Networks (ISN), Xidian University, China. His research interests include semantic and pragmatic communication, reconfigurable intelligent surface aided joint communication and sensing in coal mines, deep learning technologies for wireless communications, etc. He is also serving as a review editor in Frontiers in Space Technologies and Frontiers in Computer Science. He has served as workshop co-chair of ICSINC Big Data Workshop 2021. He has reviewed papers from IEEE Wireless Communications and Wireless Communications and Mobile Computing.

Xianzhong Li received the B.S. degree in science and technology of electronic information from Shanxi University in 2020, where he is currently pursuing the M.S. degree in information and communication engineering.

Muyu Mei received the B.S. degree in applied mathematics from the Xidian University in 2017, where he is currently pursuing the Ph.D. degree in information and communication systems. His research interests include performance analysis and stochastic optimization for large-scale wireless networks and multihop ad hoc networks.

Zhaohui Yang (S'14-M'18) received the B.S. degree in information science and engineering from Chien-Shiung Wu Honors College, Southeast University, Nanjing, China, in June 2014, and the Ph.D. degree in communication and information system with the National Mobile Communications Research Laboratory, Southeast University, Nanjing, China, in May 2018. From 2018 to 2020, he was a postdoctoral research associate with the Center for Telecommunications Research, Department of Informatics, King's College London, UK. From 2020 to 2022, he was a research fellow with the Department of Electronic and Electrical Engineering, University College London, UK. He is currently a ZJU young professor with the College of Information Science and Electronic Engineering Zhejiang Key Lab of Information Processing Communication and Networking, Zhejiang University, and also a research scientist with Zhejiang Lab. He is an Associate Editor for the IEEE Communications Letters, IET Communications and EURASIP Journal on Wireless Communications and Networking. He has guest edited a feature topic of IEEE Communications Magazine on Communication Technologies for Efficient Edge Learning and a special issue of Journal on Selected Areas in Communications for Beyond Transmitting Bits: Context, Semantics and Task-Oriented Communications. He was a Co-Chair for international workshops with more than 10 times including ICC, GLOBECOM, WCNC, PIMRC, INFOCOM. His research interests include joint communication, sensing, and computation, federated learning, reconfigurable intelligent surface, UAV, and NOMA. He was a TPC member of IEEE ICC during 2015-2022 and GLOBECOM during 2017-2022. He was an exemplary reviewer for IEEE Transactions on Communications in 2019 and 2020.

Jia Shi (Member, IEEE) received the M.Sc. and Ph.D. degrees from the University of Southampton, U.K., in 2010 and 2015, respectively. From 2015 to 2017, he was a Research Associate with Lancaster University, U.K. From 2017 to 2018, he became a Research Fellow with 5GIC, University of Surrey, U.K. Since 2018, he has been with Xidian University, China, where he is currently an Associate Professor with the National Key Laboratory of Integrated Services Networks (ISN). His current research interests include resource allocation in wireless systems, covert communications, physical layer security, mmWave communications, and satellite communications. He is also serving as an Associate Editor for Electronic Letters, and an Editor for International Journal of Communications System. He is serving as a Guest Editor for China Communications.

Kai-Kit Wong (M'01-SM'08-F'16) received the BEng, the MPhil, and the PhD degrees, all in Electrical and Electronic Engineering, from the Hong Kong University of Science and Technology, Hong Kong, in 1996, 1998, and 2001, respectively. After graduation, he took up academic and research positions at the University of Hong Kong, Lucent Technologies, Bell-Labs, Holmdel, the Smart Antennas Research Group of Stanford University, and the University of Hull, UK. He is Chair in Wireless Communications at the Department of Electronic and Electrical Engineering, University College London, UK. His current research centers around 5G and beyond mobile communications. He is a co-recipient of the 2013 IEEE Signal Processing Letters Best Paper Award and the 2000 IEEE VTS Japan Chapter Award at the IEEE Vehicular Technology Conference in Japan in 2000, and a few other international best paper awards. He is Fellow of IEEE and IET and is also on the editorial board of several international journals. He is the Editor-in-Chief for IEEE Wireless Communications Letters since 2020.

Zhaoyang Zhang (Senior Member, IEEE) received the Ph.D. degree from Zhejiang University, Hangzhou, China, in 1998.,He is currently a Qiushi Distinguished Professor at Zhejiang University. He has coauthored more than 300 peer-reviewed international journals and conference papers, including eight conference best papers awarded by IEEE ICC 2019 and IEEE GlobeCom 2020. His research interests include fundamental aspects of wireless communications and networking, such as information theory and coding theory, network signal processing and distributed learning, AI-empowered communications and networking, and synergetic sensing, computing, and communication. He was awarded the National Natural Science Fund for Distinguished Young Scholars by NSFC in 2017. He is serving or has served as an Editor for IEEE Transactions on Wireless Communications, IEEE Transactions on Communications, and IET Communications, and the General Chair, the TPC Co-Chair, or the Symposium Co-Chair for PIMRC 2021 Workshop on Native AI Empowered Wireless Networks, VTC-Spring 2017 Workshop on HMWC, WCSP 2013/2018, Globecom 2014 Wireless Communications Symposium. He was also a Keynote Speaker for APCC 2018 and VTC-Fall 2017 Workshop NOMA.